CFD-DEM modeling the effect of column size and bed height on minimum fluidization velocity in micro fluidized beds with Geldart B particles

Yupeng Xu[a,*], Tingwen Li[a,b], Jordan Musser[a], Xiaoxing Liu[c], Guangwen Xu[c], William A. Rogers[a]

a. National Energy Technology Laboratory, Morgantown, WV 26505, USA

b. AECOM, Morgantown, WV 26505, USA

c. State Key Laboratory of Multiphase Complex Systems, Institute of Process Engineering, Chinese Academy of Sciences, Beijing 100190, P. R. China

* Corresponding author at: National Energy Technology Laboratory, Morgantown, WV 26505, USA. Tel.: 1 304 285 5462.

E-mail addresses: yupeng.xu@netl.doe.gov, yxuatnl@gmail.com

Abstract

The fluidization behavior of Geldart B particles in micro fluidized beds is investigated numerically using Computational Fluid Dynamics coupled with Discrete Element Method (CFD-DEM) available in the open-source Multiphase Flow with Interphase eXchanges (MFIX) code. The effects of different bed inner diameters (D) of 8 mm, 12 mm, 16 mm and various initial static bed heights (H) were examined. It is found that both decreasing the column diameter and increasing the bed height in a micro fluidized bed increases the minimum fluidization velocity (Umf). The observed overshoot in pressure drop that occurs before the onset of fluidization decreases in magnitude with increasing column diameter, however there is less sensitivity to bed height. Overall, the numerical results agree qualitatively with existing theoretical correlations and experimental studies. The simulations show that both column diameter and particle-wall friction contribute to the variation in minimum fluidization velocity. These two factors are coupled and hard to separate. The detailed influences of wall friction on minimum fluidization velocity are then investigated for a prescribed column diameter of 8 mm by varying the wall friction from 0 to 0.4.

Key words: micro fluidized beds; wall effect; CFD-DEM; minimum fluidization velocity; pressure overshoot

1. Introduction

Micro fluidized beds (MFBs) were first put forward by Potic et al. [1] to refer to fluidized beds with inner diameters of a few millimeters. These are ideal systems to study because they have a large wall area per unit reactor volume which promotes excellent mass- and heat-transfer. Additionally, smaller systems allow for measurement of small quantities of solid reactants. Applications of micro-fluidized beds include the Micro Fluidized Bed Reaction Analyzer (MFBRA) [2–11] and Micro Membrane Fluidized Bed Reactor (MMFBR)[12–18].

The fluidization characteristics of a given kind of particles in MFBs are different from those in the ordinary-size fluidized beds due to much stronger wall effects. From the viewpoint of operating and controlling a MFB kinetic analyzer, knowing the minimum fluidization and minimum bubbling velocities (Umf and Umb) enables researchers to determine suitable gas velocities so that fluidization in the MFB reactor can be maintained. Limited research has been conducted to understand the fundamental hydrodynamics of micro-fluidized beds.

Potic et al. [1] investigated the fluidization characteristics of liquid-solid fluidized beds with inner diameters of 1, 12 and 26 mm under high temperature and pressure conditions. Their experimental results showed that the ratio of inner bed diameter to particle diameter should be greater than 12 to ensure homogeneous fluidization that occurs at large scale. Doroodchi et al. [19] examined bed size effects on the hydrodynamics of liquid-solid MFBs in terms of minimum fluidization velocity, bed expansion, and pressure drop. Their experimental data indicates that minimum fluidization velocity increases with decreasing bed diameter. They attributed these results to a significant increase in bed voidage with a decrease in bed diameter. Li et al. [20] studied single bubble behavior in gas-liquid-solid MFBs. Their results revealed that the wall effect has a remarkable influence on bubble size. The decrease in suspension

inertial forces due to the wall effect was proposed as the contributing factor leading to the diminution of bubble size.

As for gas-solid MFB system, Liu et al. [21] conducted a series of experiments to evaluate size effects on fluidization characteristics. Their results showed that both the minimum fluidization and minimum bubbling velocities increased with decreasing bed diameters. Enhanced particle-wall frictional interaction was suggested to be the major factor responsible for the delayed onset of fluidization. Guo et al. [22] found that for gas-solid MFBs, the minimum fluidization velocity also increased with the increase of static bed height. Based on experimental results, they proposed an empirical correlation for predicting minimum fluidization velocity in gas-solid MFBs. Wang et al. [23,24] examined the fluidization behavior of FCC particles in mini- and micro- channels ranging from 700-5000 μm. They observed a regime transition instability in which there existed particulate fluidization through bubbling/slugging transition. They also found that for a given superficial gas velocity the maximum stable bubble size decreased with decreasing channel size. Recently, Vanni et al.[25] studied wall effects on the fluidization of a very dense powder (density of 19300 kg/m3) at both ambient and high temperature by decreasing the column diameter from 5 to 2 cm. They found that the wall effect only appeared in the column with a 2 cm diameter. This was evidenced by an increase in the hysteretic behavior of the pressure drop curves, an increase of the minimum fluidization velocity, and a decrease in the bed voidage after fluidization.

There exist several models to predict minimum fluidization velocity in small-scale fluidized beds by accounting for the wall effect. Di Felice and Gibilaro [26] described a method for predicting minimum fluidization and pressure drop across a particle bed by accounting for column diameter effect. They considered the column to be comprised of two sections: an inner core where the voidage remains nearly constant, and an outer annular section where the voidage varies because of the wall. Rao et al. [27] developed a model which incorporates Janssen’s wall effect in the force balance during fluidization. In their model,

the horizontal stresses acting at the wall are assumed to be a function of the local vertical stress and velocity which leads to a modified Ergun’s equation. The effect of column diameter and static bed height on minimum fluidization velocity was validated against experimental measurements.

Currently, experimental research on micro-fluidized beds hydrodynamics is limited mainly to the characterization of minimum fluidization/bubbling velocity and bed expansion. This is because fluidization characteristics of micro-fluidized beds, such as local voidage and particle velocities, are difficult to measure precisely using existing experimental techniques, such as optical fiber and capacitance probes, because of their severe interference effects. With significant improvements in high-performance computers and advances in numerical techniques and algorithms, computational fluid dynamics (CFD) has become a powerful tool for investigating the complex phenomena occurring in gas–solid fluidized beds. CFD simulations can provide massive spatial and temporal information on hydrodynamic properties without disturbing the investigated multiphase flow.

Many numerical studies have reported the performance of fluidized bed systems, however only limited work has been reported on micro-fluidized beds. Liu et al. [28] investigated fluidization behavior of Geldart A particles in a gas–solid micro-fluidized bed by Eulerian–Eulerian numerical simulations. They indicated that wall boundary conditions need to be specified carefully when gas–solid micro-fluidized beds are modeled. Recent work reported the importance of wall friction through comparison between Two Fluid model (TFM) and experiments [29–31]. Another approach, Computational Fluid Dynamics coupled with the Discrete Element Method (CFD-DEM) is a suitable tool to study the MFBs. This is because particle displacement and particle-particle and particle-wall collisions are accounted for to fully capture the wall effect which are approximated in the EE model using various closures. In CFD-DEM particle motion is computed by means of Newton's second law where collisional forces and gas particle interaction are deterministically computed. Wang et al. [32] and Tan

et al. [33,34] employed CFD-DEM to study the Micro Membrane Fluidized Bed Reactor (MMFBR). Galvin and Benyahia [35] numerically studied the effects of van der Waals type cohesive forces in the fluidization and defluidization of Group A powders in a micro-fluidized bed. They reported that cohesive forces are necessary to fully exhibit the role friction plays in commonly observed phenomena, such as pressure overshoot and hysteresis around minimum fluidization.

In this paper, CFD-DEM is employed to investigate the influence of different column diameters and bed heights on the minimum fluidization behavior of Geldart B particles. This paper is organized as follows. The numerical model is summarized in section 2 and simulation details are provided in section 3. Results and discussion are presented in Section 4. Finally, conclusions and future work are provided.

2. Simulation methods

In this study, the Multiphase Flow with Interphase eXchanges (MFIX) code, available from the U.S. Department of Energy (DOE), National Energy Technology Laboratory (NETL) at https://mfix.netl.doe.gov, was used. MFIX is a general-purpose computer code for modeling the hydrodynamics, heat transfer and chemical reactions in fluid-solids systems. In MFIX-DEM, a CFD flow solver is coupled with a DEM to simulate gas–solid flow [36–40]. Gas flow is modeled by the averaged Navier–Stokes equations for mass and momentum conservation, while the motion of particles is described by the well –established Newton’s equations of motion. The MFIX-DEM governing equations and key closure models used in this work are detailed below.

2.1. Equations of motion for the particles

In DEM, the position and linear and angular velocities of each particle are tracked. The translational and rotational motion of particle i with mass m_i, moment of inertia I_i and coordinate r_i can be described by Newton's equations for rigid body motion

$$m_i \frac{\mathrm{d}^2 \mathbf{r}_i}{\mathrm{d}t^2} = \mathbf{F}_{g,i} + \mathbf{F}_{c,i} + \mathbf{F}_{p,i} + \mathbf{F}_{d,i} \quad (1)$$

$$I_i \frac{\mathrm{d}\omega_i}{\mathrm{d}t} = \mathbf{T}_i \quad (2)$$

The four terms on the right-hand side of (1) account for the gravitational force, the sum of the individual contact forces exerted by all other particles in contact with particle i, the pressure gradient force induced by the pressure difference, and the drag force induced by the relative velocity between the particles and local gas velocity, respectively. In (2), ω_i is the angular velocity and T_i is the torque around the center-of-mass of particle i due to particle collision forces. Two types of collision models are widely used, namely the hard sphere model and the soft sphere model. In our simulation, the soft sphere model is used since the hard sphere model is not suited for systems where quasi static particle configurations exist, more detailed information can be found in [41–44].

For the calculation of $\mathbf{F}_{c,i}$, a linear spring and dashpot soft-sphere collision model along the lines of Cundall and Strack is used [45,46]. In this model, the total contact force on particle i of radius R_i is given by a sum of normal and tangential pair forces with neighboring particles in contact,

$$\mathbf{F}_{c,i} = \sum_{j \in contactlist} (\mathbf{F}_{n,ij} + \mathbf{F}_{t,ij}) \quad (3)$$

The normal forces $\mathbf{F}_{n,ij}$ between two particles i and j can be calculated by

$$\mathbf{F}_{n,ij} = -k_n \delta_n \mathbf{n}_{ij} - \eta_n \mathbf{V}_{n,ij} \quad (4)$$

where k_n is the nomal spring stiffness, η_n the normal damping coefficient. The normal force depends linearly on the overlap $\delta_n = R_i + R_j - |r_i - r_j|$ and relative normal velocity $\mathbf{v}_{n,ij} = (\mathbf{v}_{ij} \cdot \mathbf{n}_{ij})\mathbf{n}_{ij}$, where $\mathbf{n}_{ij}$ is

the unit vector pointing from the center of j to the center of i, and $\mathbf{v}_{ij}$ is the relative velocity of particles i and j, which is

$$\mathbf{v}_{ij} = (\mathbf{v}_i - \mathbf{v}_j) + (R_i\boldsymbol{\omega}_i + R_j\boldsymbol{\omega}_j) \times \mathbf{n}_{ij} \quad (5)$$

Where $\mathbf{v}_i$ and $\mathbf{v}_j$ are particles velocities, $\boldsymbol{\omega}_i$ and $\boldsymbol{\omega}_j$ the angular velocities.

The tangential component of the contact force is given as

$$\mathbf{F}_{t,ij} = \begin{cases} -k_t\delta_t\mathbf{t}_{ij} - \eta_t\mathbf{V}_{t,ij} & \text{for } |\mathbf{F}_{t,ij}| \le \mu_f |\mathbf{F}_{n,ij}| \\ -\mu_f |\mathbf{F}_{n,ij}| \mathbf{t}_{ij} & \text{for } |\mathbf{F}_{t,ij}| > \mu_f |\mathbf{F}_{n,ij}| \end{cases} \quad (6)$$

Note that k_t is the tangential spring stiffness, δ_t is the tangential displacement, η_t is the tangential damping coefficient, $\mathbf{v}_{t,ij}$ is the tangential relative velocity, μ_f is the friction coefficient, and $\mathbf{t}_{ij}$ is the tangential unit vector. The tangential relative velocity is

$$\mathbf{V}_{t,ij} = \mathbf{V}_{ij} - \mathbf{V}_{n,ij} \quad (7)$$

and the tangential unit vector t_{ij} is defined as

$$\mathbf{t}_{ij} = \frac{\mathbf{V}_{t,ij}}{|\mathbf{V}_{t,ij}|} \quad (8)$$

The tangential forces also lead to a torque force on the particles:

$$\mathbf{T}_i = \sum_{j \in contactlist} (R_i\mathbf{n}_{ij} \times \mathbf{F}_{t,ij}) \quad (9)$$

The pressure gradient force $\mathbf{F}_{p,i}$ is evaluated as

$$\mathbf{F}_{p,i} = -\nabla P_g(\mathbf{x}_i) V_i \quad (10)$$

Where V_i is the total volume of particle i and ∇P_g stands for the local pressure gradient of the gas phase across the particle i.

$\mathbf{F}_{d,i}$ is the gas phase drag force exerted on particle i given by

$$\mathbf{F}_{d,i} = \frac{\beta_i V_i}{\varepsilon_s}(\mathbf{v}_g(\mathbf{x}_i) - \mathbf{u}_i) \tag{11}$$

where ε_s is the solids volume fraction in the computational cell in which the particle is located. $\mathbf{v}_g$ and $\mathbf{u}_i$ are the gas phase and solid phase velocity vectors in the cell and β_i is the interphase momentum exchanging coefficient for particle i, which is calculated using the empirical correlation proposed by Gidaspow [47]

$$\beta_i = \begin{cases} 150\dfrac{\varepsilon_s(1-\varepsilon_g)\mu_g}{\varepsilon_g(d_i\phi_s)^2} + 1.75\dfrac{\varepsilon_s\rho_g\left|\mathbf{v}_g(\mathbf{x}_i) - \mathbf{u}_i\right|}{d_i\phi_s} & \text{if } \varepsilon_g < 0.8 \\ \dfrac{3}{4}C_{D,i}\varepsilon_g^{-2.65}\dfrac{\varepsilon_s\varepsilon_g\rho_g\left|\mathbf{v}_g(\mathbf{x}_i) - \mathbf{u}_i\right|}{d_i\phi_s} & \text{if } \varepsilon_g < 0.8 \end{cases} \tag{12}$$

$$C_{D,i} = \begin{cases} \dfrac{24}{\mathrm{Re}_i\,\varepsilon_g}(1 + 0.15(\mathrm{Re}_i\,\varepsilon_g)^{0.687}) & \text{if } \mathrm{Re}_i\,\varepsilon_g < 1000 \\ 0.44 & \text{if } \mathrm{Re}_i\,\varepsilon_g \geq 1000 \end{cases} \tag{13}$$

$$\mathrm{Re}_i = \frac{\rho_g\left|\mathbf{v}_g(x_i) - \mathbf{u}_i\right| d_i\phi_s}{\mu_g} \tag{14}$$

where ϕ_s is the sphericity of the particles accounting for the particles shape.

2.2. Governing equations for the gas phase

The gas phase flow field is computed from the volume-averaged Navier–Stokes equations given by:

$$\frac{\partial}{\partial t}(\varepsilon_g\rho_g) + \nabla\cdot(\varepsilon_g\rho_g\mathbf{u}_g) = 0 \tag{15}$$

$$\frac{\partial}{\partial t}(\varepsilon_g \rho_g \mathbf{u}_g) + \nabla \cdot (\varepsilon_g \rho_g \mathbf{u}_g \mathbf{u}_g) = -\varepsilon_g \nabla p - \nabla \cdot (\varepsilon_g \tau_g) - \mathbf{S}_p + \varepsilon_g \rho_g \mathbf{g} \quad (16)$$

where ε_g is the local gas volume fraction, ρ_g is gas phase density, u_g is gas velocity, p is gas pressure, τ is viscous stress tensor, g is gravitational acceleration, and s_p is a source term which accounts for the momentum exchange with the solid particles and it is computed from:

$$\mathbf{S}_p = \frac{1}{V} \sum_{i=1}^{n} \frac{\beta_i V_i}{\varepsilon_s} (\mathbf{v}_g(\mathbf{x}_i) - \mathbf{u}_i) \quad (17)$$

The fluid density is determined using the ideal gas law, and the viscous stress tensor is assumed to obey the general form for a Newtonian fluid.

$$\tau_g = -\left[(\lambda_g - \frac{2}{3}\mu_g)(\nabla \cdot \mathbf{u}_g)\mathbf{I} + \mu_g((\nabla \mathbf{u}_g) + (\nabla \mathbf{u}_g)^{\mathbf{T}}) \right] \quad (18)$$

Full details on the governing equations along with the numerical implementation and coupling procedure can be found in Garg et al. [36,37].

3. Simulation settings

In the current simulations, cylindrical fluidized beds with different column sizes and static bed heights were investigated and influences on minimum fluidization velocity were studied. A schematic of the bed is shown in Fig. 1. Gas enters the column from the bottom with a prescribed inlet velocity and exits the system through a pressure outlet on the top. No-slip wall boundary condition is used for the gas phase. The bed was comprised of 550μm diameter and density of 2500 kg/m3 glass bead particles which were previously tested experimentally. Simulation conditions and physical properties of the gas and solids are listed in Table 1.

Column diameters (D) of 0.80 cm, 1.28 cm, 1.60 cm were simulated using grid dimensions of three times the particle diameter. The MFIX Cartesian grid cut-cell technique was used to specify the geometry. In this approach, a Cartesian grid is used to discretize the

computational domain while boundary cells are truncated to conform to the domain surface. Details on the Cartesian grid cut-cell method can be found in Kirkpatrick et al. [48]. The MFIX Cartesian grid cut-cell implementation is described by Dietiker [49] and Dietiker et al. [50]. Simulations were run in hybrid parallel mode by coupling distributed memory parallel (DMP) and shared memory parallel (SMP) using message passing interface (MPI) and open multi-processing (OpenMP) on NETL's supercomputer [51,52].

Fig. 1.

The simulation procedure goes as follows:

Step 1, particles were generated inside the column then settle under gravity.

Step 2, the bed was slowly fluidized then defluidized to generate a random close–packing state which eliminated the influence of the initial packing due to uniform particle seeding.

Step 3, the formal runs starts and results are recorded for analysis.

During step 2 and 3, the inlet velocity was slowly increased beyond the point of fluidization and then decreased to zero to obtain the entire pressure drop profile. The inlet velocity was increased at rates of 1and 2 cm/s2 respectively to mimic experimental procedure for measuring minimum fluidization velocity [21,27]. There was no noticeable difference between 1 and 2 cm/s2 (not shown here), thus 1 cm/s was used in all subsequent simulations. A characteristic pressure drop profile (both fluidization and defluidization) using 550 μm particles in the 0.8 cm diameter column is shown in Fig. 2.

Table 1

Fig. 2.

As shown in Fig. 2, pressure drop across the bed increases as inlet gas velocity is increased. Shortly after gas velocity exceeds minimum fluidization velocity, Umf, the pressure drop reaches a maximum value before fluctuating around a mean value. Once the bed is fully

fluidized, U_g is slowly decreased to zero to obtain the pressure drop profile for defluidization. It can be seen from Fig. 2 that the defluidization curve is smoother than the fluidization curve which is consistent with experimental observations. In Fig. 2 the maximum value of the pressure drop is defined as P_{max}, the average pressure drop of the fluidized bed is defined as $\overline{P}$, and the weight of the fluidized particles in the bed of unit cross-sectional area is defined as mg/A. As we can see, both P_{max} and $\overline{P}$ are greater than mg/A. To facilitate analyses, we define the difference between the pressure drop across the bed when the particles are fully fluidized and the weight of the particles as:

$$\Delta P = \overline{P} - \frac{mg}{A} \tag{19}$$

The pressure drop overshoot before fluidization is consistent with that reported in the experimental work by [21]. Here the difference between the maximum pressure drop and the pressure due to the weight of the particles is defined as:

$$\Delta P_{\max} = P_{\max} - \frac{mg}{A} \tag{20}$$

The defluidization curve was used to determine minimum fluidization velocity for different conditions. Minimum fluidization velocity is defined as the intersection point between the fixed bed pressure drop curve during defluidization and the average pressure drop of the fluidized bed as indicated in Fig. 2.

4. Results and discussion

4.1 Effect of column diameter

Experiments have shown that both column diameter [21,27] and static bed height [27] influence minimum fluidization velocity for small-scale fluidized beds. In the current study, both effects are investigated. Fig. 3 shows variations in minimum fluidization velocity (noted as Umf hereafter) under three column diameters for a prescribed

bed height of 6.88 cm. Umf is normalized by the value calculated by the Ergun equation [53] for the bulk region where wall effects are absent. In addition to these values, two existing correlations by Rao et al. [27] and Di Felice & Gibilaro [26] are drawn for comparison.

Fig. 3.

The simulation results show Umf decreasing with increasing column diameters. This is in qualitative agreement with the experimental results and correlations by Rao et al. [27] and Di Felice & Gibilaro [26]. As we see from this figure, simulated values do not match the correlations. The relative deviations between the predicted Umf and the reference correlation of Rao et al.[27] are 9.4%, 8.4% and 5.1% for 3 different column diameters, while the relative deviations between the predicted Umf and the reference correlation of Di Felice & Gibilaro [26] are 5.7% and 1.9% for column diameters of 1.28 cm and 1.60 cm. This is attributed to the different mechanisms assumed in the two correlations. As mentioned before, the increase of Umf in MFBs is generally attributed to two mechanisms: an increase of bed voidage due to the boundary wall geometrical effect [19] , and enhanced particle-wall frictional interaction due to an increase in the ratio of particle-wall contact surface area to the bulk volume [21]. The correlation proposed by Di Felice and Gibilaro [26] assumes fluidization delay is due to the former, while the model of Rao et al. [27] assumes the later. In real MFB systems, both mechanisms are like to contribute. Better agreement between simulation values and the correlation of Rao et al. [27] for relatively large D/d suggest that the frictional effect may be the dominate factor. Conversely, simulation results agree better with Di Felice's correlation [26] for small D/d hinting that the geometrical effect is likely more important.

The Di Felice's minimum fluidization correlation is written as:

$$U_{mf} = U_b(2.06 - 1.06(\frac{(D/d)-1}{(D/d)})^2) \qquad 21$$

The wall effect is only expected at small column diameter (D) to particle diameter (d) ratios, where U_b is the minimum fluidization velocity of bulk region. Different experimental results [21,27] at even larger ratios have shown that this correlation underestimates the wall effect.

The solids volume fractions of the settled bed after defluidization in different column diameters are shown in Table 2. The solids volume fraction increases with increasing column diameters, which contributes to the decrease of the minimum fluidization velocity.

Table 2

Rao et al.’s correlation considers the particle-wall frictional interaction as the main wall effect. As a result, a greater effect is expected for smaller column diameters because the ratio of particle-wall contact surface area increases with decreasing column diameter. The total particle-wall tangential force normalized by the weight of the bed is shown in Fig. 4 for the different column diameters. For clarity, only the forces during defluidization are shown. In this figure, we can see that when the particles inside the column are fully fluidized and slugging occurs, the total tangential force is negative, in alignment with gravity. This explains why the pressure drop is greater than bed weight during fluidization in Fig. 2. While the particles are defluidized, the total tangential force is positive to partially support the bed weight. From this figure, we can see that the column wall provides support to defluidize particles leading to large voidage inside the settled bed. The fraction of bed weight supported by the wall decreases with the increasing column diameter. The change in packing density close to the wall is usually attributed to the geometrical effect. In this regard, particle-wall friction further enhances the geometrical effect. Hence, these two factors, frictional and geometrical effects from the wall, are coupled and hard to distinguish. The influence of particle-wall tangential forces for a prescribed column diameter, especially when the particle-wall friction coefficient are different, are discussed in the next section.

Fig. 4.

4.2 Effect of static bed height

Liu et al. [21] investigated the influence of different bed heights on minimum fluidization velocity with particle diameters of 96.4 μm, 242.1 μm, 460.6 μm. Their results showed that there is a small effect for larger particles. Similarly, Rao et al. [27]'s experimental results showed that the effect of bed height on Umf is important for micro fluidized beds. The influence of bed height on Umf for similar particles as used by Rao et al. [27] are shown in Fig. 5. Here, Rao's correlation is provided in addition to simulation results. The overall simulation results trend agree well with Rao's correlation, however simulation Umf values are slightly lower than the correlation. The relative deviations between the predicted Umf and the reference correlation of Rao et al. [27] are 2.8%, 1.4%, 2.5%, 1.5%,3.8% and 1.4%.

Fig. 5.

Another interesting feature is the pressure drop overshoot that occurs just before fluidization. This feature commonly exist both for type A and type B powders in the Geldart classification. In 1993, Tsinontides and Jackson [54] observed pressure drop overshoot through beds of FCC particles (Geldart A). Pressure drop overshoot has since been studied by many other researchers. For type A particles, coexistence of cohesive forces, particle-particle and particle-wall friction forces, and the interplay between cohesive and friction forces make it very difficult to distinguish the cause of the overshoot. Past experimental work and simulation studies have come to different conclusions [35,54–58].

Type B particles are more appropriate for studying this phenomenon because the pressure overshoot still exists while cohesive forces are relatively small. Both Liu et al. [21] and Rao et al. [27]'s experimental work showed pressure overshoot for Geldart B particles. Loezos et al. [58] found that pressure overshoot in gas-solid

fluidization is attributed primarily to wall effects and the overshoot extent generally decreases with increasing bed sizes. This behavior was explained by suggesting an additional force is needed to dislodge interlocking coarser particles such as uniformly sized sharp sand. The current study uses cohesiveless, spherical type B particles to study wall effect which excludes any particle shape effect.

Fig. 6 shows the pressure difference of ΔP_{max} and ΔP for a 6.88 cm bed height and varying column diameters. Both decrease with increasing column diameter and are more prominent at smaller column diameters when wall effect is more important. Compared with ΔP, ΔP_{max} is larger at smaller column diameters while the difference between ΔP and ΔP_{max} diminishes at larger column diameters. This suggests that the overshoot only exists for small column diameters which agrees with the findings of Loezos et al. [58].

Fig. 6.

Influence of bed height on pressure difference is shown in Fig. 7 for a column diameter D=1.6 cm and varying bed heights, H. Here, the difference between ΔP and ΔP_{max} is small for shallow beds and increases with increasing bed height. Overall, the difference between ΔP and ΔP_{max} is relatively small for the 1.6 cm column diameter. Ideally, a linear relationship is expected if the wall effect scales with bed height. The current simulation results suggest a slight non-linear behavior with respect to bed height which would be of interest for future study. Similar trends were obtained for smaller column diameters.

Fig. 7.

We conclude from these results that, even without cohesive forces, pressure overshoot and Umf variation still exist for Geldart B particles. As previously mentioned, the wall effect is two-fold and can be attributed primarily to wall effects and tangential forces between particles and the wall. First, the presence of wall leads to a

slightly lower packing density as indicated in Table 2. Second, the wall frictional force tends to prevent particles from moving during fluidization and impedes particle settling during defluidization. Both effects are coupled and hard to distinguish.

4.3 Parametric study of wall friction

As shown in previous results, geometrical effect and wall friction are coupled and hard to separate. However, it is possible to evaluate their individual influence in simulations. Here, the frictional effect is investigated by varying the particle-wall friction coefficient $\mu_{p\text{-}w}$ from 0.0 to 0.4 for the 0.8 cm bed diameter and 6.88 cm static bed height. The fluidization curves for different particle-wall friction coefficients are shown in Fig. 8. When particle-wall friction is equal to zero, there is no noticeable pressure overshoot which is consistent with the above analysis. As the particle-wall friction coefficient increases, both the overshoot and average bed pressure drop during fluidization increase. The detailed pressure difference under different particle-wall friction coefficients are shown in Fig. 9. Both pressure differences increase with increasing particle-wall friction.

Fig. 8.

Fig. 9.

The total tangential force between particles and wall during defluidization are shown in Fig. 10 under different particle-wall friction coefficients. When the bed is defluidized to a settled state, the tangential force is positive indicating the wall partially supports the weight of particles. The tangential force at the settled state, Ug = 0, increases with an increasing particle-wall friction coefficient and converges for coefficients greater than 0.3. The particle-wall tangential force is negative during fluidization indicating upward particle movement which is consistent with slugging observed in simulations. Again, tangential force magnitude during fluidization increases with particle-wall friction coefficient.

Fig. 10.

The effect of particle-wall friction on settled solids packing is examined in Fig. 11. The solid volume fraction decreases from 0.634 to 0.614 when particle-wall friction coefficient is increased from 0 to 0.4. The increased porosity in the packed bed leads to less resistance to flow, ie. gas-solid drag, hence delays in fluidization. This is illustrated by calculating minimum fluidization velocities from the Ergun equation using predicted packing densities given in Fig. 11. The Ergun equation and simulation prediction for Umf agree well for zero friction suggesting that the Ergun equation captures the drag force reasonably well. However, differences between Umf calculated from Ergun equation and values predicted from simulations increase with increasing friction coefficient. This is attributed to a higher pressure drop than the bed weight during the fluidization state when wall friction is present. As shown in Fig. 2, minimum fluidization velocity is defined as the intersection point between the pressure drop during defluidization and the mean pressure drop during fluidization. This is different from the theoretical prediction which equates the pressure drop from Ergun equation to the bed weight. The elevated pressure drop due to wall friction further delays the onset of fluidization for the studied system.

Fig. 11.

Conclusions

The current study investigates minimum fluidization velocity and pressure drop of Geldart’s group B particles in micro-fluidized beds with different column diameters and bed heights using CFD-DEM simulations. Consistent with reported experimental work and theoretical correlations, decreasing bed column diameters and increasing bed height increase the wall effect in micro fluidized beds. This leads to an increased minimum fluidization velocity and larger pressure difference between the actual pressure drop and the pressure due to the particle weight. The pressure drop overshoot prior to fluidization observed in simulations is found to decrease in magnitude

with increasing column diameter. These simulation results show that both boundary wall geometrical effect and particle-wall friction contribute to a delay in fluidization in micro fluidized beds. These two factors are strongly coupled and hard to isolate. The wall frication effect was examined for a 0.8 cm bed diameter by varying the particle-wall friction coefficient. It is found that the wall friction mainly affects particle packing leading to higher minimum fluidization velocities. Additionally, wall friction during fluidization leads to a pressure drop greater than the bed weight which further increases minimum fluidization velocity.

In this study, the CFD-DEM is demonstrated to be a very powerful tool to investigate fluidization characteristics of micro-fluidized beds. Future work will build on this work and focus on flow hydrodynamics and mixing in micro-fluidized beds.

Acknowledgements

This technical effort was performed in support of the U.S. Department of Energy, Office of Fossil Energy's Advanced Numerical Simulation of Multiphase Flow through the National Energy Technology Laboratory under the RES contract DE-FE0004000. This research was also supported in part by an appointment to the National Energy Technology Laboratory Research Participation Program, sponsored by the U.S. Department of Energy and administered by the Oak Ridge Institute for Science and Education

Disclaimer

trademark, manufacturer, or otherwise does not necessarily constitute or imply its endorsement, recommendation, or favoring by the United States Government or any agency thereof. The views and opinions of authors expressed herein do not necessarily state or reflect those of the United States Government or any agency thereof.

References

[1] B. Potic, S.R.A. Kersten, M. Ye, M.A. van der Hoef, J.A.M. Kuipers, W.P.M. van Swaaij, Fluidization with hot compressed water in micro-reactors, Chem. Eng. Sci. 60 (2005) 5982–5990.

[2] J. Yu, J. Yue, Z. Liu, L. Dong, G. Xu, J. Zhu, Z. Duan, L. Sun, Kinetics and mechanism of solid reactions in a micro fluidized bed reactor, AIChE J. 56 (2010) 2905–2912.

[3] J. Yu, X. Zeng, J. Zhang, M. Zhong, G. Zhang, Y. Wang, G. Xu, Isothermal differential characteristics of gas–solid reaction in micro-fluidized bed reactor, Fuel. 103 (2013) 29–36.

[4] F. Wang, X. Zeng, Y. Wang, H. Su, J. Yu, G. Xu, Non-isothermal coal char gasification with CO2 in a micro fluidized bed reaction analyzer and a thermogravimetric analyzer, Fuel. 164 (2016) 403–409.

[5] F. Wang, X. Zeng, R. Shao, Y. Wang, J. Yu, G. Xu, Isothermal Gasification of in Situ / ex Situ Coal Char with CO 2 in a Micro Fluidized Bed Reaction Analyzer, Energy & Fuels. 29 (2015) 4795–4802.

[6] F. Wang, X. Zeng, Y. Wang, J. Yu, Characterization of coal char gasification with steam in a micro-fluidized bed reaction analyzer, Fuel Process. Technol. 141 (2016) 2–8.

[7] Y. Zhang, G. Sun, S. Gao, G. Xu, Regeneration Kinetics of Spent FCC Catalyst via Coke Gasification in a Micro Fluidized Bed, Procedia Eng. 102 (2015) 1758–1765.

[8] Y. Zhang, M. Yao, S. Gao, G. Sun, G. Xu, Reactivity and kinetics for steam gasification of petroleum coke blended with black liquor in a micro fluidized bed, Appl. Energy. 160 (2015) 820–828.

[9] J. Yu, X. Zeng, G. Zhang, J. Zhang, Y. Wang, G. Xu, Kinetics and Mechanism of Direct Reaction between CO 2 and Ca(OH) 2 in Micro

Fluidized Bed, Environ. Sci. Technol. 47 (2013) 7514–7520.
[10] Y. Song, Y. Wang, W. Yang, C. Yao, G. Xu, Reduction of NO over biomass tar in micro-fluidized bed, Fuel Process. Technol. 118 (2014) 270–277.
[11] X. Zeng, F. Wang, Y. Wang, A. Li, J. Yu, G. Xu, Characterization of Char Gasification in a Micro Fluidized Bed Reaction Analyzer, Energy & Fuels. 28 (2014) 1838–1845.
[12] N.T.Y. Dang, F. Gallucci, M. van Sint Annaland, Micro-structured fluidized bed membrane reactors: Solids circulation and densified zones distribution, Chem. Eng. J. 239 (2014) 42–52.
[13] L. Roses, F. Gallucci, G. Manzolini, S. Campanari, M. van Sint Annaland, Comparison between fixed bed and fluidized bed membrane reactor configurations for PEM based micro-cogeneration systems, Chem. Eng. J. 171 (2011) 1415–1427.
[14] M.A. Rakib, J.R. Grace, C.J. Lim, S.S.E.H. Elnashaie, B. Ghiasi, Steam reforming of propane in a fluidized bed membrane reactor for hydrogen production, Int. J. Hydrogen Energy. 35 (2010) 6276–6290.
[15] N.T.Y. Dang, F. Gallucci, M. van Sint Annaland, Influence of Reactor and Particle Scale on the Hydrodynamics of Microstructured Fluidized Bed Membrane Reactors, Ind. Eng. Chem. Res. 52 (2013) 18192–18205.
[16] T.Y.N. Dang, F. Gallucci, M. van Sint Annaland, Gas back-mixing study in a membrane-assisted micro-structured fluidized bed, Chem. Eng. Sci. 108 (2014) 194–202.
[17] N.T.Y. Dang, F. Gallucci, M. van Sint Annaland, An experimental investigation on the onset from bubbling to turbulent fluidization regime in micro-structured fluidized beds, Powder Technol. 256 (2014) 166–174.
[18] T.Y.N. Dang, F. Gallucci, M. van Sint Annaland, Gas mixing study in freely bubbling and turbulent gas–solid fluidized beds with a novel infrared technique coupled with digital image analysis, Chem. Eng. Sci. 116 (2014) 38–48.
[19] E. Doroodchi, Z. Peng, M. Sathe, E. Abbasi-Shavazi, G.M. Evans, Fluidisation and packed bed behaviour in capillary tubes, Powder

Technol. 223 (2012) 131–136.
[20] Y. Li, M. Liu, X. Li, Single bubble behavior in gas–liquid–solid mini-fluidized beds, Chem. Eng. J. 286 (2016) 497–507.
[21] X. Liu, G. Xu, S. Gao, Micro fluidized beds: Wall effect and operability, Chem. Eng. J. 137 (2008) 302–307.
[22] Q. j. Guo, Y. Xu, X. Yue, Fluidization Characteristics in Micro-Fluidized Beds of Various Inner Diameters, Chem. Eng. Technol. 32 (2009) 1992–1999.
[23] F. Wang, L.-S. Fan, Gas–Solid Fluidization in Mini- and Micro-channels, Ind. Eng. Chem. Res. 50 (2011) 4741–4751.
[24] F. Wang, L.S. Fan, Gas-Solid Fluidization in a Microfluidic Channel, in: 13th Int. Conf. Fluid. - New Paradig. Fluid. Eng., 2010.
[25] F. Vanni, B. Caussat, C. Ablitzer, M. Brothier, Effects of reducing the reactor diameter on the fluidization of a very dense powder, Powder Technol. 277 (2015) 268–274.
[26] R. Di Felice, L.G. Gibilaro, Wall effects for the pressure drop in fixed beds, Chem. Eng. Sci. 59 (2004) 3037–3040.
[27] A. Rao, J.S. Curtis, B.C. Hancock, C. Wassgren, The effect of column diameter and bed height on minimum fluidization velocity, AIChE J. 56 (2010) 2304–2311.
[28] X. Liu, C. Zhu, S. Geng, M. Yao, J. Zhan, G. Xu, Two-fluid modeling of Geldart A particles in gas–solid micro-fluidized beds, Particuology. 21 (2015) 118–127.
[29] Y. Zhao, B. Lu, Y. Zhong, Influence of collisional parameters for rough particles on simulation of a gas-fluidized bed using a two-fluid model, Int. J. Multiph. Flow. 71 (2015) 1–13.
[30] L.M. Garcia-Gutierrez, F. Hernández-Jiménez, E. Cano-Pleite, A. Soria-Verdugo, Improvement of the simulation of fuel particles motion in a fluidized bed by considering wall friction, Chem. Eng. J. 321 (2017) 175–183.
[31] L. (Lei) Yang, J.T. (Johan) Padding, J.A.M. (Hans) Kuipers, Modification of kinetic theory of granular flow for frictional spheres, part II: Model validation, Chem. Eng. Sci. 152 (2016)

783–794.
[32] J. Wang, L. Tan, M.A. van der Hoef, M. van Sint Annaland, J.A.M. Kuipers, From bubbling to turbulent fluidization: Advanced onset of regime transition in micro-fluidized beds, Chem. Eng. Sci. 66 (2011) 2001–2007.
[33] L. Tan, I. Roghair, M. van Sint Annaland, Simulation study on the effect of gas permeation on the hydrodynamic characteristics of membrane-assisted micro fluidized beds, Appl. Math. Model. 38 (2014) 4291–4307.
[34] L. Tan, I. Roghair, M. van Sint Annaland, Discrete particle simulations of micro membrane-assisted fluidized beds with H2 extraction, Int. J. Hydrogen Energy. 41 (2016) 8719–8731.
[35] J.E. Galvin, S. Benyahia, The effect of cohesive forces on the fluidization of aeratable powders, AIChE J. 60 (2014) 473–484.
[36] R. Garg, J. Galvin, T. Li, S. Pannala, Open-source MFIX-DEM software for gas–solids flows: Part I—Verification studies, Powder Technol. 220 (2012) 122–137.
[37] T. Li, R. Garg, J. Galvin, S. Pannala, Open-source MFIX-DEM software for gas-solids flows: Part II — Validation studies, Powder Technol. 220 (2012) 138–150.
[38] M. Syamlal, W. Rogers, T.J. O’brien, Summary of MFIX Equations, 2012.
[39] M. Syamlal, MFIX Documentation: Numerical Technique, 1998.
[40] M. Syamlal, W. Rogers, T.J. O’brien, MFIX Documentation: Theory Guide, 1993.
[41] B.J. Alder, T.E. Wainwright, Phase Transition for a Hard Sphere System, J. Chem. Phys. 27 (1957) 1208–1209.
[42] M.A. van der Hoef, M. Ye, M. van Sint Annaland, A.T. Andrews, S. Sundaresan, J.A.M. Kuipers, Multiscale Modeling of Gas-Fluidized Beds, Adv. Chem. Eng. 31 (2006) 65–149.
[43] Y. Xu, J.T. Padding, M.A. van der Hoef, J.A.M. Kuipers, Detailed numerical simulation of an intruder impacting on a granular bed using a hybrid discrete particle and immersed boundary (DP-IB) method, Chem. Eng. Sci. 104 (2013) 201–207.

[44] Y. Xu, J.T. Padding, J.A.M. Kuipers, Numerical investigation of the vertical plunging force of a spherical intruder into a prefluidized granular bed, Phys. Rev. E. 90 (2014) 62203.
[45] M. van Sint Annaland, N.G. Deen, J.A.M. Kuipers, Numerical simulation of gas–liquid–solid flows using a combined front tracking and discrete particle method, Chem. Eng. Sci. 60 (2005) 6188–6198.
[46] Q. Xiong, B. Li, G. Zhou, X. Fang, J. Xu, J. Wang, X. He, X. Wang, L. Wang, W. Ge, J. Li, Large-scale DNS of gas–solid flows on Mole-8.5, Chem. Eng. Sci. 71 (2012) 422–430.
[47] D. Gidaspow, Multiphase flow and fluidization: Continuum and kinetic theory descriptions, Academic Press, New York, 1994.
[48] M.P. Kirkpatrick, S.W. Armfield, J.H. Kent, A representation of curved boundaries for the solution of the Navier–Stokes equations on a staggered three-dimensional Cartesian grid, J. Comput. Phys. 184 (2003) 1–36.
[49] J.F. Dietiker, C. Guenther, M. Syamlal, A Cartesian Cut Cell Method for Gas/Solids Flow, in: AIChE Annu. Meet., Nashville, TN, 2009.
[50] J.F. Dietiker, Multiphase Flow with Interphase eXchanges: Cartesian Grid User Guide, 2015.
[51] H. Liu, D.K. Tafti, T. Li, Hybrid parallelism in MFIX CFD-DEM using OpenMP, Powder Technol. 259 (2014) 22–29.
[52] P. Gopalakrishnan, D. Tafti, Development of parallel DEM for the open source code MFIX, Powder Technol. 235 (2013) 33–41.
[53] S. Ergun, Fluid flow through packed columns, Chem. Eng. Prog. 48 (1952) 89–94.
[54] S.C. Tsinontides, R. Jackson, The mechanics of gas fluidized beds with an interval of stable fluidization, J. Fluid Mech. 255 (1993) 237–274.
[55] J.M. Valverde, A. Ramos, A. Castellanos, P. Keith Watson, The tensile strength of cohesive powders and its relationship to consolidation, free volume and cohesivity, Powder Technol. 97 (1998) 237–245.

[56] Jackson R., The nature and role of effective stress in fluidized systems., in: Fluid. IX, Engineering Foundation Publication, New York, 1998: pp. 1–13.

[57] R. Jackson, The Dynamics of Fluidized Particles, Cambridge University Press, 2000.

[58] P.N. Loezos, P. Costamagna, S. Sundaresan, The role of contact stresses and wall friction on fluidization, Chem. Eng. Sci. 57 (2002) 5123–5141.

List of figure captions

Fig. 1. Schematic representation of the micro fluidized bed

Fig. 2. Example of a pressure drop profile (both fluidization and defluidization) using particles of D = 550 μm in the 0.8 cm diameter column with a static bed height of 6.88 cm

Fig. 3. Influence of the column diameters on the minimum fluidization velocity (static bed height of 6.88 cm)

Fig. 4. Normalized tangential force of different column diameters (static bed height of 6.88 cm)

Fig. 5. Influence of different bed heights on the minimum fluidization velocity with column diameter of 1.6 cm

Fig. 6. Influence of the column diameters on the pressure difference (static bed height of 6.88 cm)

Fig. 7. Influence of the bed height on the pressure difference (column diameter of 1.6 cm)

Fig. 8. Fluidization curves under different particle-wall frictions (column diameter of 0.8 cm and static bed height of 6.88 cm)

Fig. 9. Pressure difference under different particle-wall friction coefficients (column diameter of 0.8cm and static bed height of 6.88 cm)

Fig. 10. The tangential force exerted on the particles by the wall (column diameter of 0.8cm and static bed height of 6.88 cm), the slugging behavior of μ=0.4 is shown as an example

Fig. 11. Minimum fluidization velocity under different particle-wall friction coefficients (column diameter of 0.8cm and static bed height of 6.88 cm)

Table 1

Table 1: Parameters used in the numerical simulations

Parameter	Unit	Value
Gravity y-direction	m/s2	9.81
Gas density	Kg/m3	1.2
Gas viscosity	Pa·s	1.8e-5

Particle diameter	µm	550
Particle density	kg/m3	2500
Particle sphericity	-	0.9
Restitution coefficient (normal)	-	0.99
Restitution coefficient (tangential)	-	0.3
Friction coefficient between particles	-	0.4
Friction coefficient between particle and wall	-	0.4
Normal spring stiffness	N/s	100

Table 2

Table 2: Solids volume fraction under different column diameters

	8.0 mm	12.8 mm	16.0 mm
ε_s	0.6143	0.6204	0.6240

Fig.1.

Click here to download high resolution image

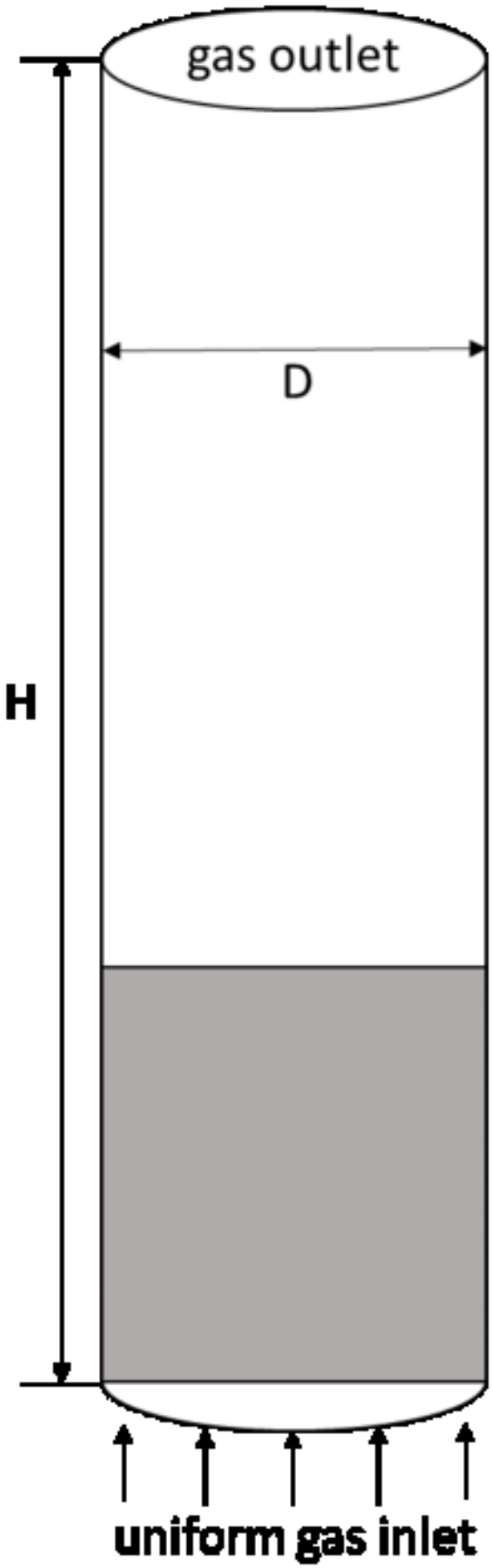

Fig.2.
Click here to download high resolution image

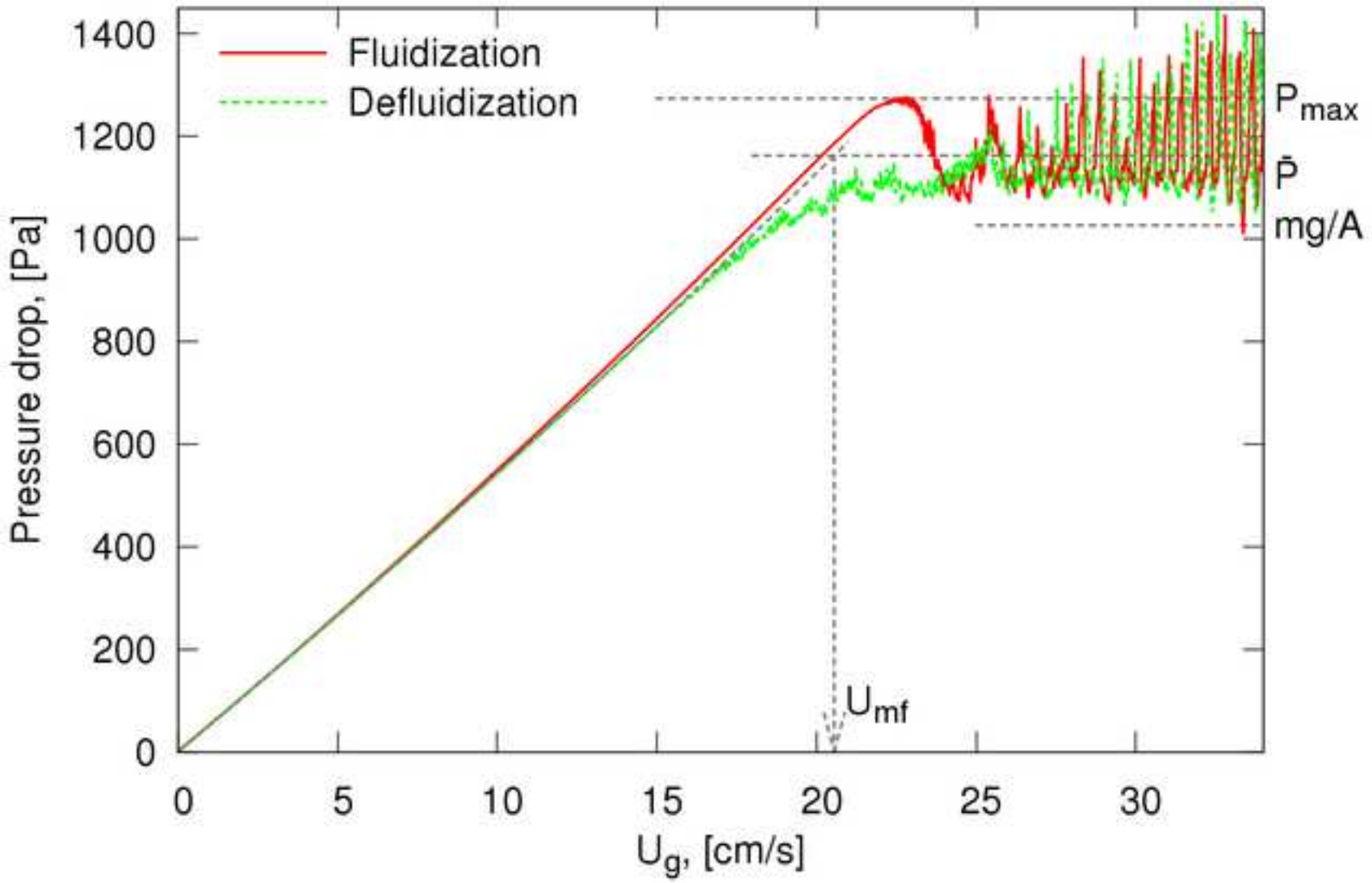

Fig.3.
Click here to download high resolution image

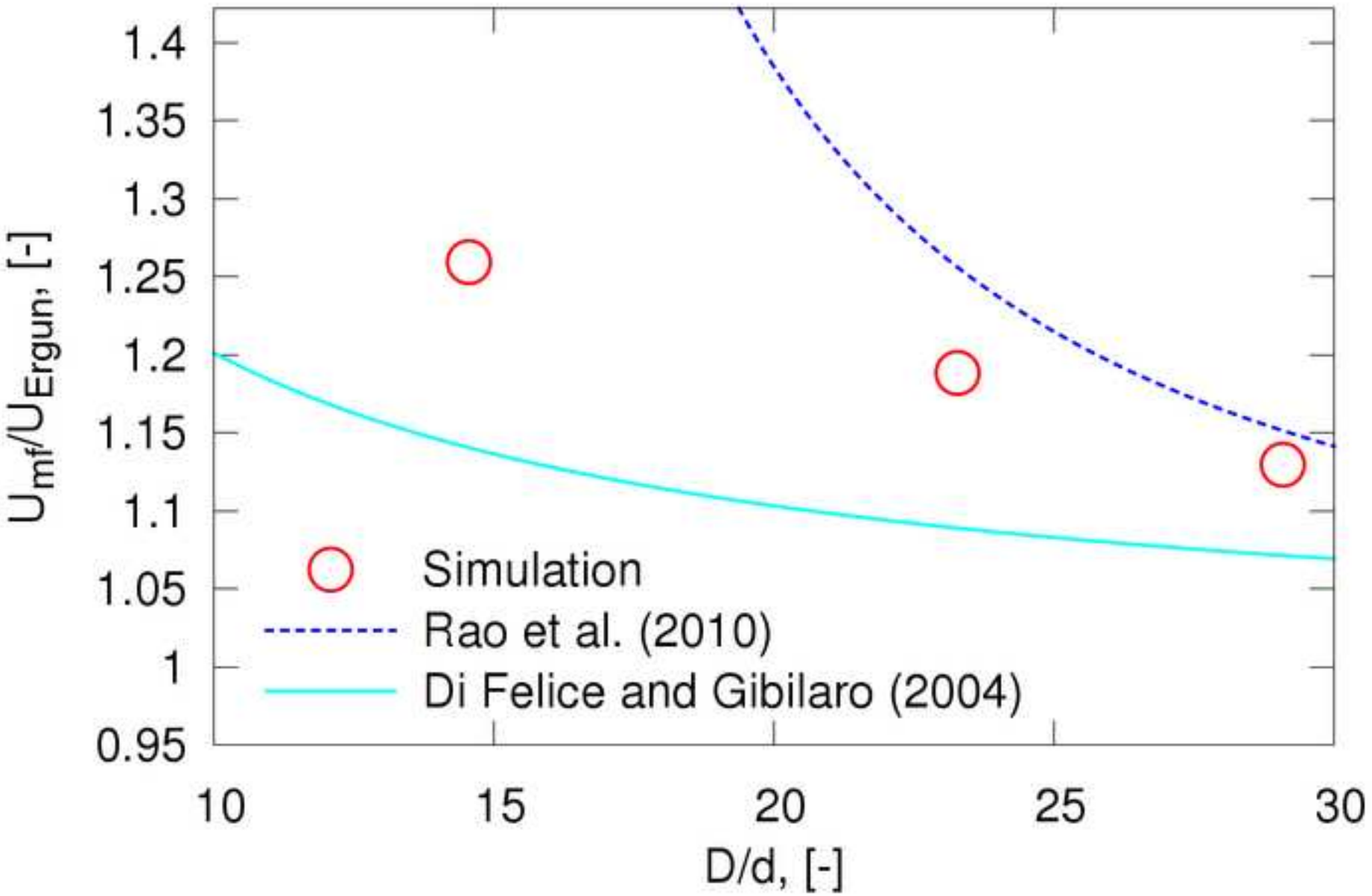

Fig.4.
Click here to download high resolution image

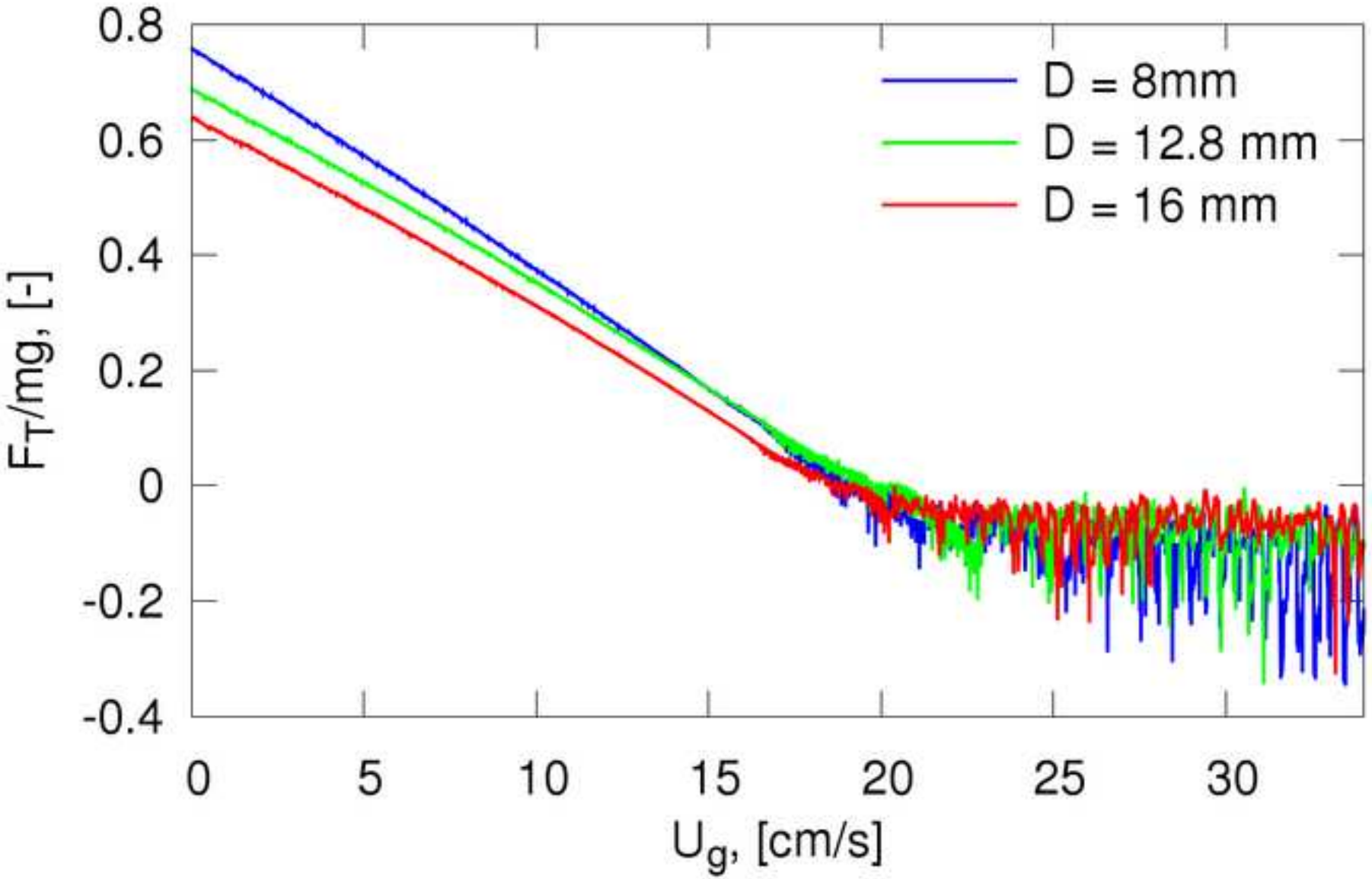

Fig.5.
Click here to download high resolution image

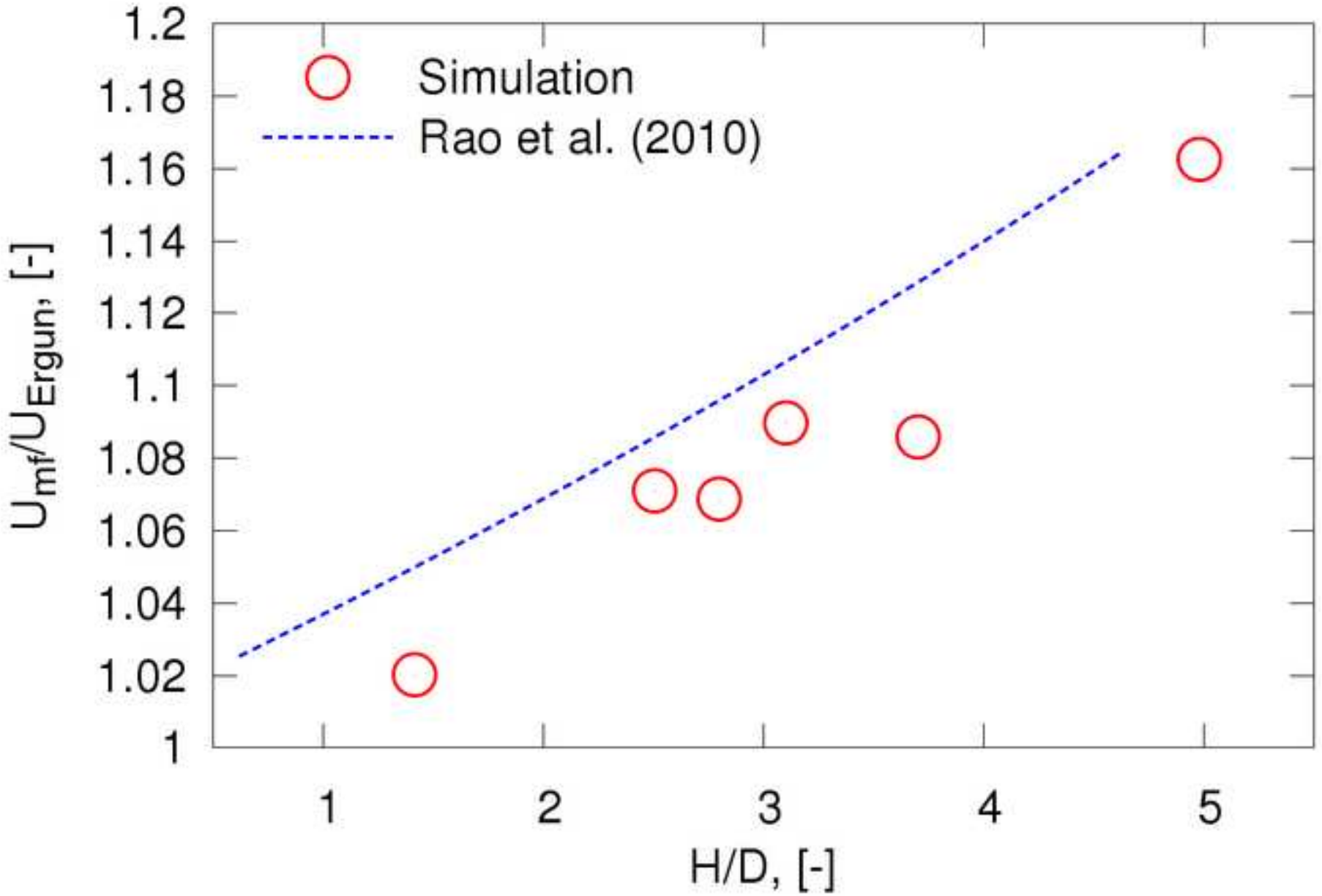

Fig.6.
Click here to download high resolution image

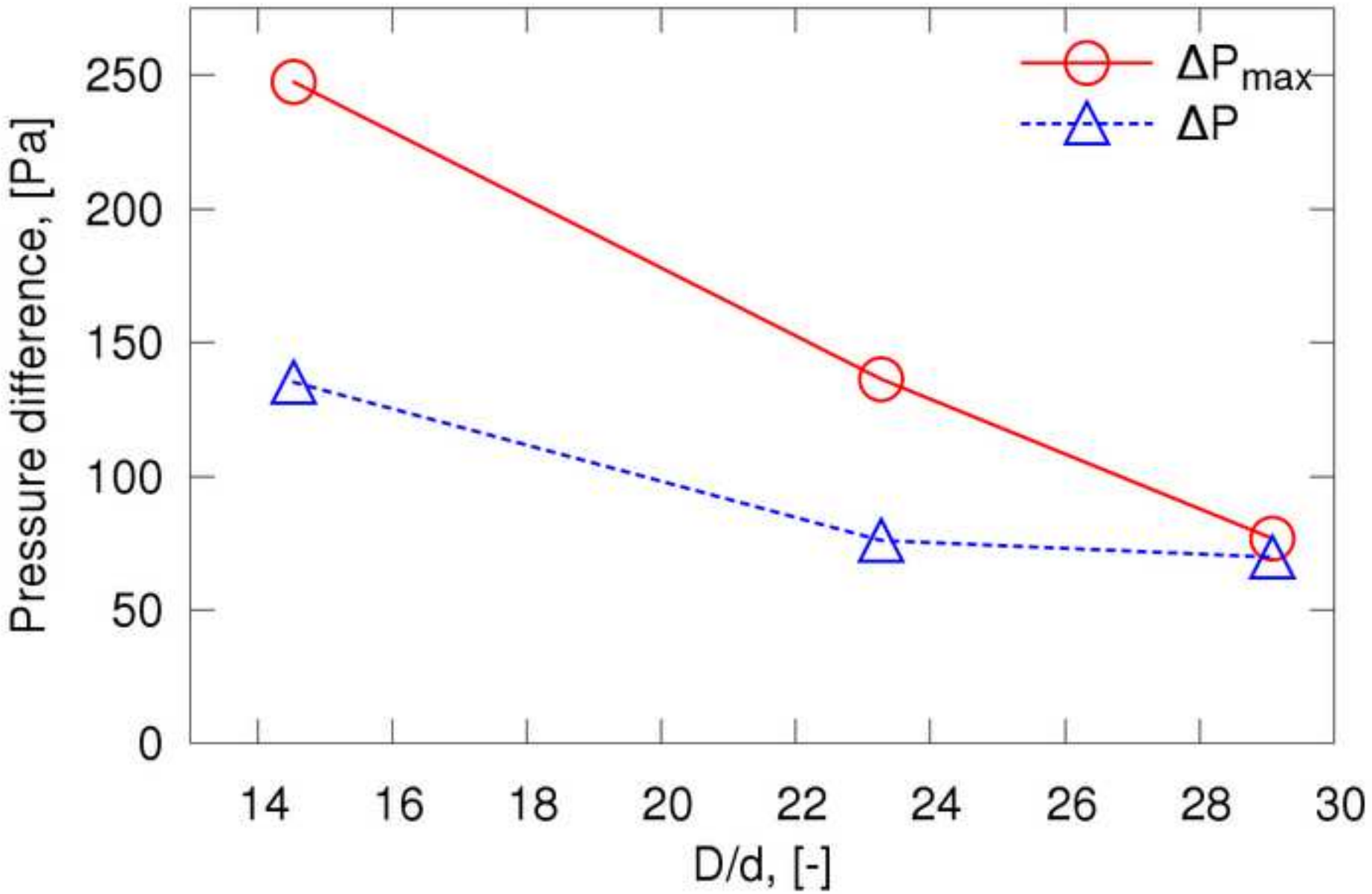

Fig.7.
Click here to download high resolution image

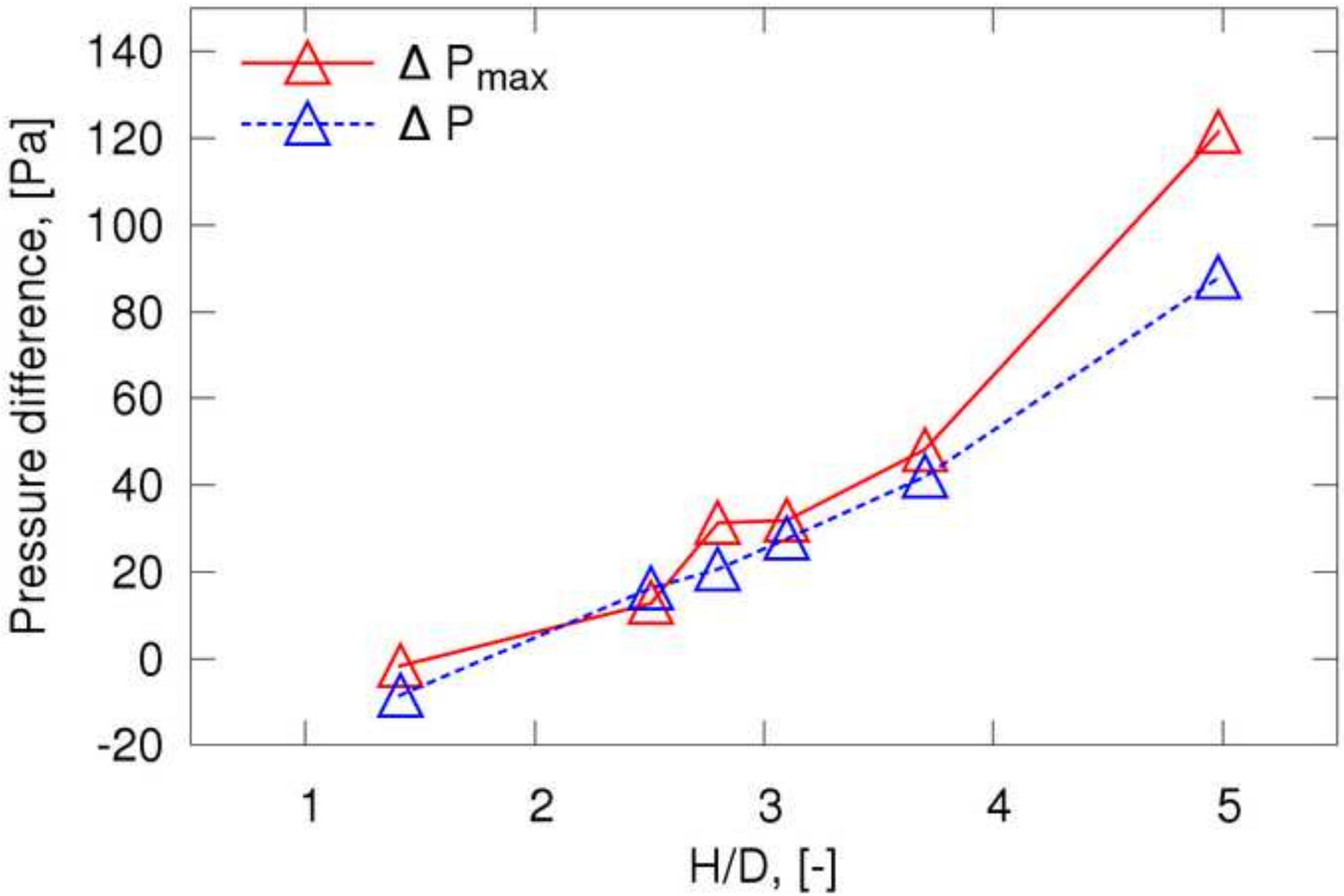

Fig.8.
Click here to download high resolution image

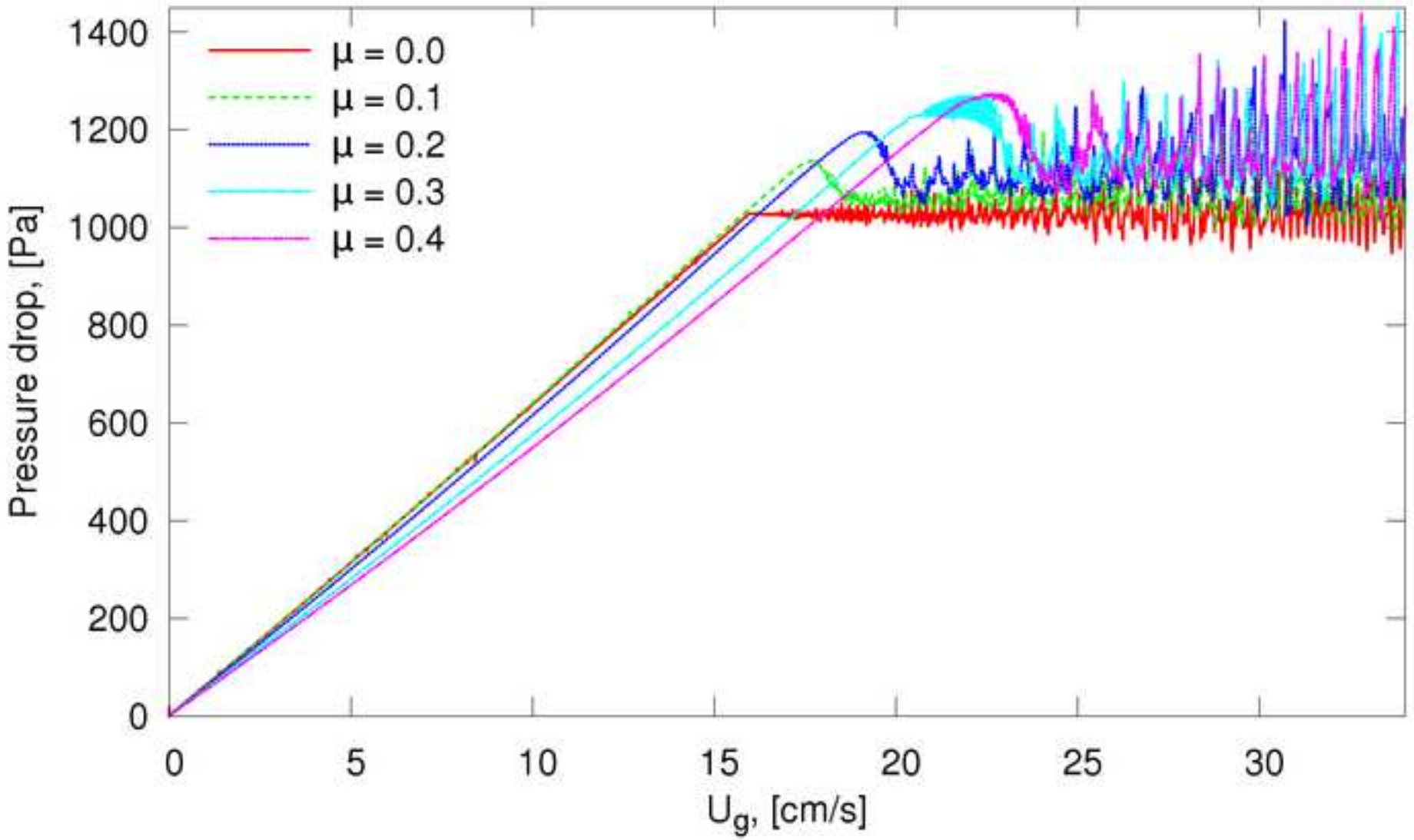

Fig.9.
Click here to download high resolution image

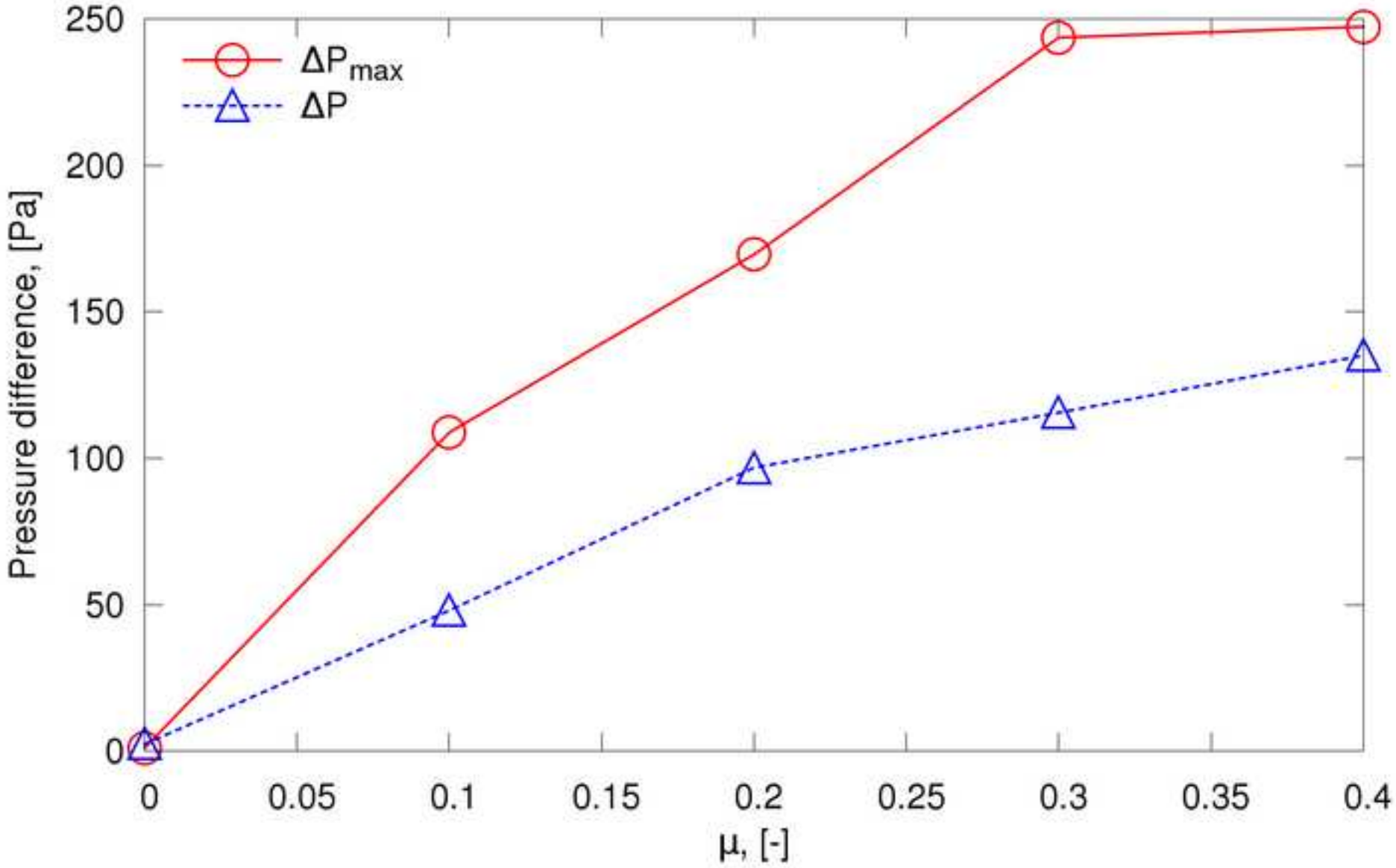

Fig.10.
Click here to download high resolution image

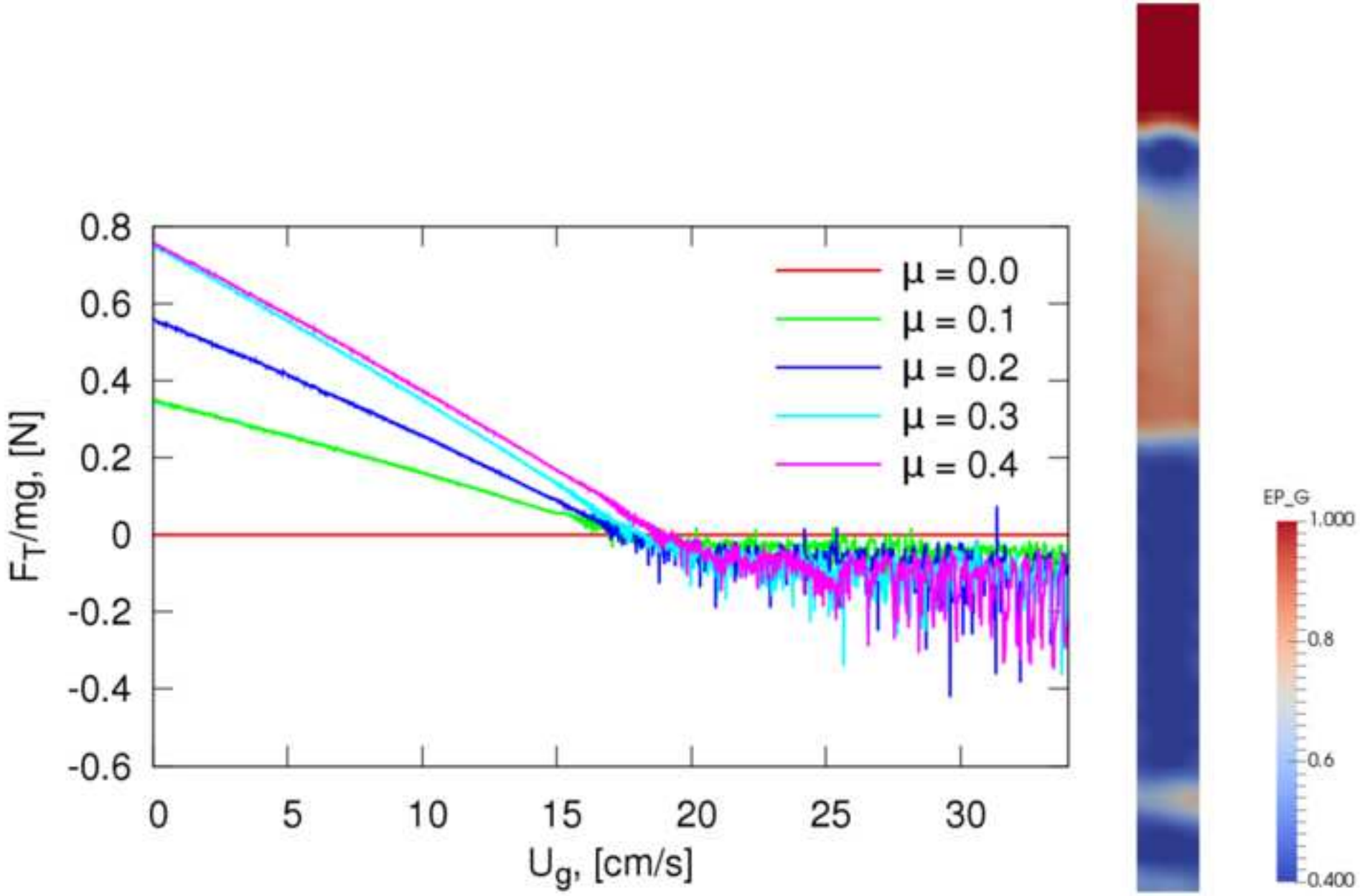

Fig.11.

Click here to download high resolution image

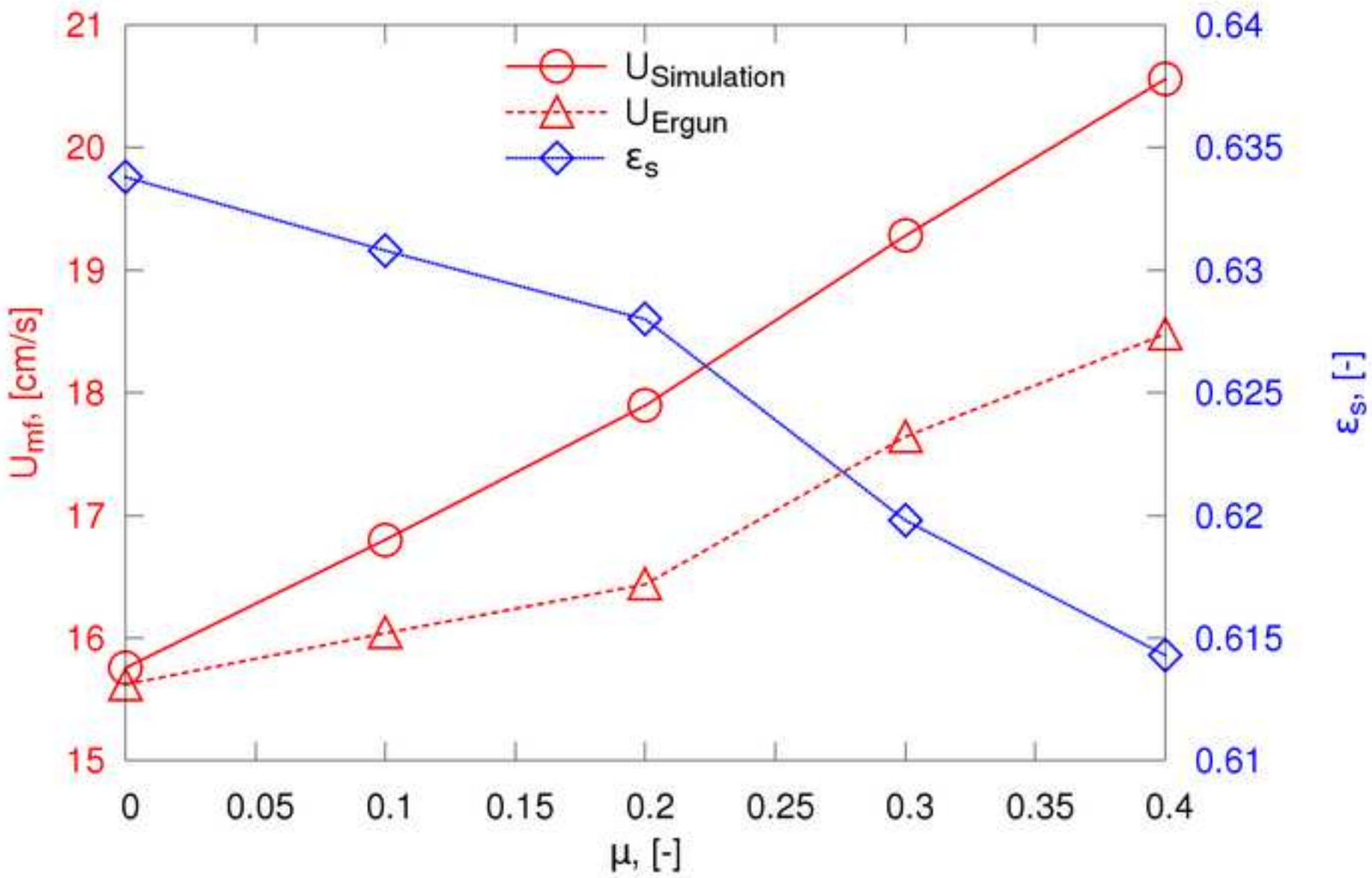

*Graphical Abstract (for review)

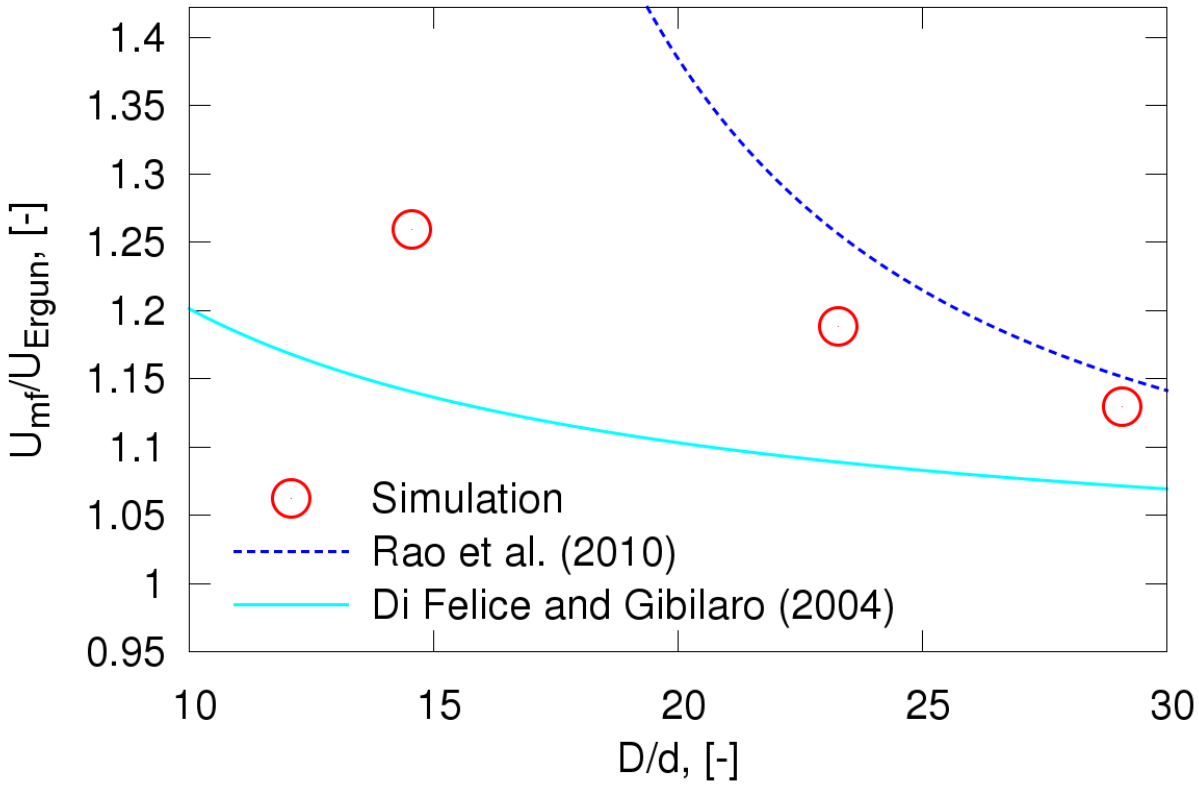

***Abstract**

The fluidization behavior of Geldart B particles in micro fluidized beds is investigated numerically using Computational Fluid Dynamics coupled with Discrete Element Method (CFD-DEM) available in the open-source Multiphase Flow with Interphase eXchanges (MFIX) code. The effects of different bed inner diameters (D) of 8 mm, 12 mm, 16 mm and various initial static bed heights (H) were examined. It is found that both decreasing the column diameter and increasing the bed height in a micro fluidized bed increases the minimum fluidization velocity (Umf). The observed overshoot in pressure drop that occurs before the onset of fluidization decreases in magnitude with increasing column diameter, however there is less sensitivity to bed height. Overall, the numerical results agree qualitatively with existing theoretical correlations and experimental studies. The simulations show that both column diameter and particle-wall friction contribute to the variation in minimum fluidization velocity. These two factors are coupled and hard to separate. The detailed influences of wall friction on minimum fluidization velocity are then investigated for a prescribed column diameter of 8 mm by varying the wall friction from 0 to 0.4.

***Highlights (for review)**

- Umf and pressure drop of Geldart B particles in micro fluidized beds were studied.
- Decreasing bed column diameters and increasing bed height increase the wall effect.
- Both boundary wall effect and particle-wall friction contribute to the wall effect.
- Wall friction mainly affects particle packing leading to higher Umf.